



**HAL**  
open science

# Flash floods triggered by the 15–17th March 2022 rainstorm event in the Atacama Desert mapped from InSAR coherence time series

Albert Cabré, Dominique Remy, Odin Marc, Katy Burrows, Sébastien  
Carretier

## ► To cite this version:

Albert Cabré, Dominique Remy, Odin Marc, Katy Burrows, Sébastien Carretier. Flash floods triggered by the 15–17th March 2022 rainstorm event in the Atacama Desert mapped from InSAR coherence time series. *Natural Hazards*, 2023, 116 (1), pp.1345-1353. 10.1007/s11069-022-05707-y . hal-04187968

**HAL Id: hal-04187968**

**<https://hal.science/hal-04187968>**

Submitted on 15 Nov 2023

**HAL** is a multi-disciplinary open access archive for the deposit and dissemination of scientific research documents, whether they are published or not. The documents may come from teaching and research institutions in France or abroad, or from public or private research centers.

L'archive ouverte pluridisciplinaire **HAL**, est destinée au dépôt et à la diffusion de documents scientifiques de niveau recherche, publiés ou non, émanant des établissements d'enseignement et de recherche français ou étrangers, des laboratoires publics ou privés.

3

4 **Flash floods triggered by the 15-17<sup>th</sup> March 2022 rainstorm event in the Atacama Desert**  
5 **mapped from InSAR coherence time series**

6 Albert Cabré<sup>a,b\*</sup>, Dominique Rémy<sup>a</sup>, Odin Marc<sup>a</sup>, Katy Burrows<sup>a</sup>, Sébastien Carretier<sup>a</sup>

7 <sup>a</sup>Geosciences Environnement Toulouse, OMP, UPS, CNRS, IRD, CNES Université de Toulouse,  
8 France

9 <sup>b</sup>Advanced Mining Technology Center, Universidad de Chile, Santiago, Chile

10 \*corresponding author: [albert.cabre@get.omp.eu](mailto:albert.cabre@get.omp.eu)

11 **Abstract**

12 This research provides examples of the impacts of flash floods of March 2022 rainstorm event on the  
13 Atacama Desert infrastructures investigated by means of InSAR coherence and in situ observations.  
14 The erosional processes associated with flash floods and the downstream distance they can travel are  
15 poorly known, preventing any mitigation strategy. Thus, a better understanding of sediment  
16 mobilization during high-intensity rainstorm events in the Atacama Desert is therefore essential to  
17 assess the impact of hydrogeomorphic hazards on critical infrastructures and ecosystems.  
18 The main findings are (i) the devastating role of small-scale (<5km radius) rainfall cells and their large  
19 impact on transport network infrastructures and, (ii) the impact on infrastructure depended mainly on  
20 the transport capacity of the flows, which is in turn determined by the drained area upstream of the  
21 considered channel, and the rainfall intensity on these upstream areas. For example, water flows with  
22 high discharge could remove larger volumes of sediments, undermining and cutting roads. Such flows  
23 were frequent at ~26°S, while at ~22°S they were limited to a few channels with large contributing  
24 areas. This resulted in extensive damage and required considerable time and money to recondition  
25 the road. In contrast, thinner mudflows with limited transport capacity tend to follow the roads and  
26 leave a thin deposit of mud that can be cleaned in a few days. The fact that roads transported  
27 mudflows over large distances and that mining infrastructure deflects natural drainages has been  
28 observed as a potential hazard to downstream infrastructures or inhabited areas.

29

30 **Keywords**

31 Flash floods, Atacama Desert, rainfall, InSAR, coherence, transport networks

32 **Acknowledgements**

33 Funding for this research was provided by the *Centre National d'Etudes Spatiales* (CNES)  
34 postdoctoral program to AC and KB, through the Programme National de Télédétection Spatiale  
35 (PNTS) project SECURITY, IRD-LMI-COPEDIM and ANID FONDECYT Iniciación Folio 11220285.  
36 Javiera Chocobar is thanked for assistance with fieldwork during the day in the Sierra Gorda area.  
37 Access to Agisoft Photoscan 1.2.4 licence is gratefully acknowledged to Stéphane Bonnet.

38 **Flash floods triggered by the 15-17<sup>th</sup> March 2022 rainstorm event in the Atacama Desert**  
39 **mapped from InSAR coherence time series**

40 **1. Introduction**

41 In arid areas such as the Atacama Desert, infrequent, high-intensity rainstorm events have triggered  
42 hydrogeomorphic hazards such as debris floods and debris flows with resulting damage to  
43 infrastructure and loss of life. In this area, recent examples of destructive flash floods and/or debris  
44 flows have been triggered by the rainstorm events of July 1991 (e.g., Vargas et al., 2000), February  
45 2001 (Mather and Hartley, 2005; Houston, 2006) and March 2015 (e.g., Wilcox et al., 2016; Cabré et  
46 al., 2020 a,b; Aguilar et al., 2020). These events resulted in high costs and economic losses due to  
47 infrastructure damage (e.g., transport networks) and were able to remobilize sediments of abandoned  
48 mine tailings with potential downstream pollution (e.g., Tapia et al., 2018; Aguilar et al., 2021). The  
49 erosional processes associated with flash floods and debris flows, the conditions for their triggering  
50 and the downstream distance they can travel are poorly known, preventing any mitigation strategy. A  
51 better understanding of sediment mobilization during high-intensity rainstorm events in a place like the  
52 Atacama Desert is therefore essential to assess the impact of hydrogeomorphic hazards on critical  
53 infrastructures and ecosystems.

54 Progress in understanding the impact of heterogeneous rainfall in arid areas has been limited by the  
55 absence of suitable high-resolution monitoring methodologies capable of tracking the sources of  
56 sediment entrainment and the places where they accumulate. The Sentinel-1 constellation, by offering  
57 an improvement in revisit time (6 days at best) over previous missions, has stimulated the  
58 development through Interferometric Synthetic Aperture Radar (InSAR) of novel protocols of surface  
59 change monitoring in the Atacama Desert. For example, a statistical analysis of long Sentinel-1  
60 coherence time series combined with optical and field data has proved to be a valuable tool to map the  
61 spatial and temporal surface change due to erosion and deposition in arid areas (Cabré et al., 2020a).  
62 This analysis allowed a clear discrimination between areas affected by transient loss of coherence  
63 caused by variations in soil moisture (Scott et al., 2017; Jordan et al., 2020) and those areas affected  
64 by a permanent loss of coherence related to the modification of the soil texture by erosion and  
65 sedimentation processes.

66 This study reports and maps ground surface modifications over the Atacama Desert triggered by the  
67 storm event of 15-17 March 2022. The cause of this rainfall event is not studied here, but it may be  
68 similar to other recent events in the same region. According to Böhm et al. (2021), the June 2017  
69 rainfall event was caused by a moisture conveyor belt. More specifically, Bozkurt et al. (2016) explain  
70 the March 2015 rainfall event by the onset of El Niño 2015/16, which provided an anomalous source of  
71 water vapour, coincident with an eastward moving cut-off low (cold front) which transported the  
72 moisture to the Atacama Desert.

73 To study erosion associated with the March 2022 event, we use field data and Sentinel-1 radar data.  
74 The short revisit time of Sentinel-1 (6 days when combining Ascending and Descending tracks)  
75 allowed a rapid evaluation of the areas potentially affected from the coherence loss in images before  
76 and after the event. Aiming at being able to link the loss of coherence with specific erosion or  
77 depositional features, a field survey was performed one month after the rain event. Direct observations  
78 were obtained using Uncrewed Airborne Vehicle (UAV) photogrammetric-derived products (Digital  
79 Surface Map and orthoimage) at selected areas. These data can assist in a rapid assessment of the  
80 damage caused to infrastructure (transport network and mine tailings) by such a rapid mobilisation of  
81 sediments in the Atacama Desert, where more than 0.7 million people live, with implication for  
82 mitigation actions. They may also contribute to augmenting the national landslide inventory  
83 (<https://portalgeominbeta.sernageomin.cl/>).

84 **2. 15-17<sup>th</sup> March 2022 rainstorm**

85 During March 15-17<sup>th</sup> 2022, the IMERG (V6) satellite-based rainfall product (Huffman et al., 2017)  
86 shows two notable precipitation cells (Fig. 1b). The accumulated precipitation map in Figure 1b shows  
87 up to 30 mm in 2.5 days for the two main precipitation cells. The rain event started in the northernmost  
88 sector (~22°S), around Sierra Gorda and Calama during the afternoon on the 15<sup>th</sup> (local time) and  
89 moved southwards reaching 26°S latitude near the town of Inca de Oro during the evening of the 16<sup>th</sup>  
90 of March. In addition, reports of hail by the local population at Inca de Oro indicate a high-intensity

91 event that the IMERG product failed to retrieve. Thus, despite its ability to provide a regional overview,  
92 the IMERG product remains prone to underestimation and under detection, especially for short rainfall  
93 events, given the irregular satellite overpass.

94 Rain gauges are scarce in the Atacama Desert and some of the datasets of Chilean public agencies  
95 are only available several months after a rain event. However, the closest Chilean Meteorological  
96 Agency (<https://climatologia.meteochile.gob.cl>) fifteen-minute rainfall intensity increment rain gauge is  
97 situated at the Calama El Loa Airport. This station indicates the onset of rainfall during the night of the  
98 15<sup>th</sup> of March at 21:26:00h (Chilean local time) with final accumulation after 2.5 days of 4.8mm.

99 This storm event illustrates how difficult it is for satellite-based and/or rain gauge networks to retrieve  
100 the location and magnitude of intense rainfall cells in the Atacama region.

### 101 **3. Methods**

102 SAR was downloaded in L1 Single Look Complex (SLC) format and processed on InSAR Scientific  
103 Computing Environment (ISCE) (Rosen et al., 2012). The processing of the InSAR coherence time  
104 series followed the methodology which has already been presented for a rainstorm event in the same  
105 region in March 2015 by Cabré et al. (2020a). The involved steps consist of (i) masking areas with  
106 permanent low coherence mainly related to anthropic activities, ponds, rivers and zones with strong  
107 aeolian sediment transport, (ii) eliminating areas with transient coherence loss due to variation in soil  
108 moisture, and, (iii) highlighting areas with permanent coherence loss due to erosion by producing a  
109 map of coherence loss based on the difference of a co-event coherence map (pre-event reference  
110 image of 2022/02/24 and the secondary image of 2022/05/31) from the mean coherence map before  
111 the event. A table with scene dates is presented in the supplementary information (SI-1).

112 Fieldwork planning focussed on populated areas and tried to avoid areas where coherence loss was  
113 likely to be due to transient soil moisture effects rather than erosion (e.g., coherence loss in flat areas).  
114 Field observations and UAV surveys were carried out between the 19-25<sup>th</sup> of April at the selected  
115 locations (Fig.1a, 2a-d). At each field station, evidence of erosion was photographed (Fig. 2e-k), and  
116 flow-types were classified according to sediment concentration to indicate the dominant flow  
117 conditions at each site following Pierson and Costa (1987) and Costa (1988). UAV surveys were  
118 performed with a DJI Phantom 4 quadcopter without using Ground Control Points. Flights were  
119 conducted between 100 and 150 m above the ground to achieve a good coverage and sufficient  
120 resolution (<0.6m). Flight surveys covered areas <1 km<sup>2</sup> of permanent change (permanent coherence  
121 loss).

### 122 **4. Results: Zones of detected ground surface changes**

#### 123 *A) Inca de Oro area: local sediment remobilisation in ephemeral streams of an alluvial plain*

124 Inca de Oro is a small town situated at (-26.755, -69.904; 1595 m asl.) on a low-dipping alluvial plain  
125 with a population of approximately 500 inhabitants whose principal economic activities are related to  
126 the mining industry. This area is presented in this report because a rain cell identified in the coherence  
127 map of figure 1d with radius <5km triggered flash floods that impacted Inca de Oro houses, solar  
128 power plants and blocked the only roads that connect the town with the other cities (Fig. 2a-b, e). Hail  
129 was reported during the 2022 March event by the inhabitants indicating a short duration and high  
130 intensity storm (Actualidad Chile, 2022). Runoff generation took only a few minutes, and the flood  
131 bores suddenly flowed through the streets of Inca de Oro (Fig. 2b). Flash floods were guided by the  
132 road network and then into the ephemeral drainage network resulting in road blockages and damage  
133 downstream (Fig. 2a), as well as damage to local houses and solar power plant stations.

134 Flash floods entrained sediments from the bed of the stream making the deposited grain-size highly  
135 variable from fine sands to gravels. The stages of the flow can be reconstructed at some channels  
136 based on field evidence: a first erosive streamflow was responsible for the incision through the alluvial  
137 plain surface, including the road network (up to 1m). At some points (Fig. 2a) paved roads became the  
138 main conduits for these flows. Later stages of the flood are represented by mudflow deposits of  
139 typically less than 5 cm thick that benefited from previous depressions or pools within the channels.  
140 The rapid deposition suggests an abrupt end to the rainfall combined with the lack of subsurface flow  
141 in the area.

142 *B) Sierra Gorda area: rainfall-triggered debris floods at catchment headwards and downstream*  
143 *transport and spreading*

144 The town of Sierra Gorda (-22.892, -69.320; 1626 m asl.) is situated at the distal zone of some  
145 coalescent alluvial fans which drain towards the south-west. This is a small town, but it serves as a  
146 hub for many people working in nearby open pit mines and solar power plants. The route that  
147 connects the coastal city of Antofagasta with Calama passes through the town and was subject to  
148 several blockages due to mudflows during the storm event (Fig. 2j). This is a critical road vital to the  
149 functioning of the mining industry (which accounts for 12.5% of the country's GDP) and for the mobility  
150 of people. This area hosts also several mine tailing deposits that are potential sources of run-off  
151 pollution during rainfall events.

152 The coherence map of figure 1e shows the effects on the ground of a NW-SE band of rainfall cells and  
153 the mobilisation of sediment in the ephemeral channels situated downstream (Fig. 2f,i). The  
154 convergence of channels activated larger channels which can be individually identified on the map.  
155 Where these flows were guided by the road network mudflows were able to travel distances of up to  
156 40 km (Fig. 1e, 2j) down the main road to the south-west of the area. Other flows reached a clay-pan  
157 which remained flooded a month later (Fig. 2k).

158 Mudflows were the main flow type identified in the channels for the Sierra Gorda alluvial fans whereas  
159 in the main channels there are evidence of both mudflows and stream flows. Mudflow deposits are  
160 present within the alluvial fan channels and in the form of crevasse-splay-like deposits. When  
161 encountering an unpaved road, mudflows used it for drainage and present thin deposits of <5cm (Fig.  
162 2h). Mudflows that reached the lower parts of the catchment and progressed throughout the main  
163 route southwards deposited thicker accumulations along almost 15 km of the route (Fig. 2j) with  
164 thicknesses up to 50 cm. These mud deposits were still wet after 1 month.

165 *C) Other consequences of erosion processes during the 2022 March rainstorm event*

166 On some hillslopes the rainfall was sufficient to cause rilling, usually clustered in a dense network.  
167 Rills exhibit a steep sidewall, widths between 10-20 cm and depths up to 30 cm. The rilled hillslopes  
168 present straight rills that extend the entire length of the hillslope from the divide to the foot-slopes (Fig.  
169 2c). Rills were observed at the hillslopes of Quebrada Turquesa (~10 km from El Salvador town) (-  
170 26.1843; -69.7058) and at Quebrada El Carrizo (-25.9; -69.73). Rills may also have formed in other  
171 remote areas, not surveyed in the field.

172 Finally, another hazard was associated with the storm event: the development of an intense dust  
173 storm (haboob) (Sutton, 1925) that impacted the town of Diego de Almagro on 16 March (Portavoz  
174 Noticias Oficial, 2022). A haboob is a wall of dust that is pushed out along the surface from a  
175 thunderstorm downdraft at high speeds. When the downburst of the March 2022 thunderstorm  
176 reached the ground, loose fine sediments were blown in an area characterised by the absence of  
177 vegetation and with a large volume of loose CaSO<sub>4</sub>-rich fine sediments available in the first  
178 centimetres of soil (*chusca* or *chuca* is the local name) (Ericksen, 1983). These episodes of aeolian  
179 sediment transport are very rare in Atacama.

180 **5. Summary**

181 This study highlights the devastating role of small-scale (<5km radius) rainfall cells in arid regions and  
182 their large impact on transport network infrastructures. For such events, coherence decrease maps  
183 help to characterise the location and impact of flash floods in ephemeral drainages that intersect  
184 infrastructure (transport networks), to discriminate between ephemeral streams that have been  
185 recently activated, i.e., during the March 2015 or May 2017 rainstorm events. Such understanding is  
186 essential for local authorities in order to anticipate and mitigate the hydrogeomorphic hazards  
187 associated with the projected increase in extreme weather events.

188 The erosion processes identified at all the studied zones impacted during the March 2022 event are  
189 similar and can be classified into mudflows, debris floods and rilling. Field characterization of the  
190 deposits led us to conclude that the impact on infrastructure depended mainly on the transport  
191 capacity of the flows, which is in turn determined by the drained area upstream of the considered  
192 channel, and the rainfall intensity on these upstream areas. For example, water flows with high  
193 discharge could remove larger volumes of sediments, undermining and cutting roads. Such flows were

194 frequent near Inca de Oro, while near Sierra Gorda they were limited to a few channels with large  
195 contributing areas. This resulted in extensive damage and required considerable time and money to  
196 recondition the road (several roads were still closed 1 month after the event). In contrast, thinner  
197 mudflows with limited transport capacity tend to follow the roads and leave a thin deposit of mud that  
198 can be cleaned in a few days. In addition, the fact that roads transported mudflows over large  
199 distances and that mining infrastructure deflects natural drainages has been observed as a potential  
200 hazard to downstream infrastructures or inhabited areas.

201 Finally, although this hydrogeomorphic disaster was less catastrophic than previous ones in this area  
202 (e.g., in March 2015), likely caused by less extreme rainfall, events like the March 2022 are expected  
203 to continue to pose a regular hazard in the area (e.g., Cabré et al., 2016; Bozkurt et al., 2018; IPCC,  
204 2021). We encourage future work to consider InSAR coherence in designing mitigation strategies to  
205 avoid the devastating consequences of rainfall events in the Atacama Desert.

## 206 **References**

207 Actualidad Chile. (2022, March 18). *Intensas lluvias y granizos en Inca de Oro, comuna de Diego de*  
208 *Almagro, región de Atacama* [Video file]. YouTube. [https://www.youtube.com/watch?](https://www.youtube.com/watch?v=CANH_rXGnGY)  
209 [v=CANH\\_rXGnGY](https://www.youtube.com/watch?v=CANH_rXGnGY)

210 Aguilar, G., Valdés, A., Cabré, A., Galdames, F. (2021). Flash floods controlling Cu, Pb, As and Hg  
211 variations in fluvial sediments of a river impacted by metal mining in the Atacama Desert. *Journal of*  
212 *South American Earth Sciences*, 109, 103290. <https://doi.org/10.1016/j.jsames.2021.103290>

213 Aguilar, G., Cabré, A., Fredes, V., Villela, B. (2020). Erosion after an extreme storm event in an arid  
214 fluvial system of the southern Atacama Desert: an assessment of magnitude, return time, and  
215 conditioning factors of erosion caused by debris flows. *Natural Hazards and Earth System Sciences*,  
216 <https://doi.org/10.5194/nhess-20-1247-2020>

217 Böhm, C., Reyers, M., Knarr, L., & Crewell, S. (2021). The role of moisture conveyor belts for  
218 precipitation in the Atacama Desert. *Geophysical Research Letters*, 48, e2021GL094372.  
219 <https://doi.org/10.1029/2021GL094372>

220 Bozkurt, D., Rondanelli, R., Garreaud, R., Arriagada, A. (2016). Impact of warmer eastern tropical  
221 Pacific SST on the March 2015 Atacama floods. *Mon. Weather Rev.* 144 (11), 4441-4460

222 Bozkurt, D., Rojas, M., Boisier, J.P., Valdivieso, J. (2018). Projected hydroclimate changes over  
223 Andean basins in central Chile from downscaled CMIP5 models under the low and high emission  
224 scenarios. *Climatic Change* 150, 131–147, [doi.org/10.1007/s10584-018-2246-7](https://doi.org/10.1007/s10584-018-2246-7)

225 Cabré, M.F., Solman, S., Nuñez, M. (2016). Regional climate change scenarios over southern South  
226 America for future climate (2080-2099) using the MM5 Model. Mean, interannual variability and  
227 uncertainties. *Atmosfera Volume 29* (1), 35-60

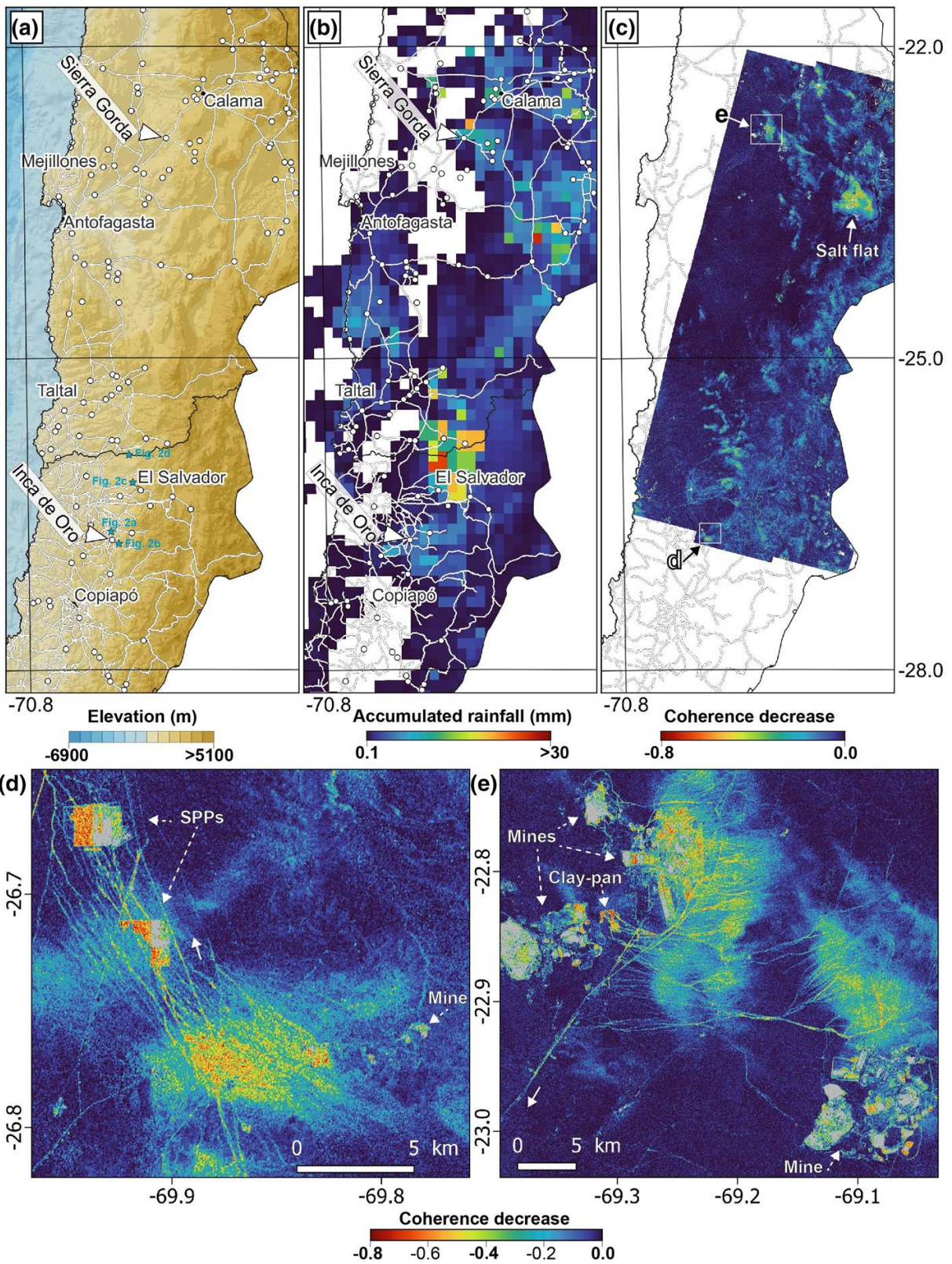
228 Cabré, A., Rémy, D., Aguilar, G., Carretier, S., Riquelme, R. (2020a). Mapping rainstorm erosion  
229 associated with an individual storm from InSAR coherence-loss validated by field evidence for the  
230 Atacama Desert. *Earth Surface Processes and Landforms*, 45 (9), 2091-2106.  
231 <https://doi.org/10.1002/esp.4868>

232 Cabré, A., Aguilar, G., Mather, A. E., Fredes, V., Riquelme, R. (2020b). Tributary-junction alluvial fan  
233 response to an ENSO rainfall event in the El Huasco watershed, northern Chile. *Progress in Physical*  
234 *Geography: Earth and Environment*, 44(5), 679-699. <https://doi.org/10.1177%2F0309133319898994>

235 Costa, J.E. (1988). Rheologic, geomorphic, and sedimentologic differentiation of water floods,  
236 hyperconcentrated flows, and debris flows. In: Baker, V.R., Kochel, R.C. & Patten, P.C. (eds) *Flood*  
237 *Geomorphology*. Wiley-Intersciences, New York, 113–122.

238 Houston, J. (2006). Variability of precipitation in the Atacama Desert: its causes and hydrological  
239 impact. *Int. J. Climatol.*, 26: 2181-2198 <https://doi.org/10.1002/joc.1359>

- 240 Huffman GJ, Bolvin DT, Braithwaite D, Hsu K, Joyce R, Kidd C, Nelkin EJ, Sorooshian S, Tan J, Xie P.  
241 (2017). Algorithm Theoretical Basis Document (ATBD) Version 4.6 for the NASA Global Precipitation  
242 Measurement (GPM) Integrated Multi-satellite Retrievals for GPM (IMERG). 32pp. GPM Project:  
243 Greenbelt, MD: [Available online at  
244 [https://pmm.nasa.gov/sites/default/files/document\\_files/IMERG\\_ATBD\\_V4.6.pdf](https://pmm.nasa.gov/sites/default/files/document_files/IMERG_ATBD_V4.6.pdf)]
- 245 IPCC (2021): Climate Change 2021: The Physical Science Basis. Contribution of Working Group I to  
246 the Sixth Assessment Report of the Intergovernmental Panel on Climate Change [Masson-Delmotte,  
247 V., P. Zhai, A. Pirani, S.L. Connors, C. Péan, S. Berger, N. Caud, Y. Chen, L. Goldfarb, M.I. Gomis, M.  
248 Huang, K. Leitzell, E. Lonnoy, J.B.R. Matthews, T.K. Maycock, T. Waterfield, O. Yelekçi, R. Yu, and B.  
249 Zhou (eds.)]. Cambridge University Press, Cambridge, United Kingdom and New York, NY, USA, 2391  
250 pp. doi:10.1017/9781009157896
- 251 Jordan, T. E., Lohman, R. B., Tapia, L., Pfeiffer, M., Scott, C. P., Amundson, R., Godfrey, L.,  
252 Riquelme, R. (2020). Surface materials and landforms as controls on InSAR permanent and transient  
253 responses to precipitation events in a hyperarid desert, Chile. *Remote Sensing of Environment*, 237,  
254 111544. <https://doi.org/10.1016/j.rse.2019.111544>
- 255 Mather, A.E. and Hartley, A.J. (2005). Flow events on a hyper-arid alluvial fan: Quebrada Tambores,  
256 Salar de Atacama, northern Chile. In: Harvey, A.M., Mather, A.E., Stokes, M. (Eds.), *Alluvial Fans:  
257 Geomorphology, Sedimentology, Dynamics*, vol. 251. Geological Society of London, Special  
258 Publications, 9-24.
- 259 Pierson, T.C. and Costa, J.E. (1987). A rheologic classification of subaerial sediment water flows.  
260 *Geol. Soc. Am. Rev. Eng. Geol.*, 7: 1-12.
- 261 Portavoz Noticias Oficial. (2022, March 17). *Tormenta de Arena en Diego de Almagro, Región de*  
262 *Atacama - 17 de marzo 2022* [Video file]. YouTube. <https://www.youtube.com/watch?v=Tt0DlooM4Yg>
- 263 Rosen, P. A., Gurrola, E., Sacco, G. F., Zebker, H. (2012). The InSAR scientific computing  
264 environment. In *EUSAR 2012; 9th European Conference on Synthetic Aperture Radar* (pp. 730–733).  
265 VDE.
- 266 Scott, C.P., Lohman, R.B., Jordan, T.E. (2017). InSAR constraints on soil moisture evolution after the  
267 March 2015 extreme precipitation event in Chile. *Sci Rep* 7, 4903 [https://doi.org/10.1038/s41598-017-](https://doi.org/10.1038/s41598-017-05123-4)  
268 [05123-4](https://doi.org/10.1038/s41598-017-05123-4)
- 269 Sutton, L.J. (1925). Haboobs. *Q.J.R. Meteorol. Soc.*, 51: 25-30.
- 270 Tapia, J., Davenport, J., Townley, B., Dorador, C., Schneider, B., Tolorza, V., von Tümpling, W.  
271 (2018). Sources, enrichment, and redistribution of As, Cd, Cu, Li, Mo, and Sb in the Northern Atacama  
272 Region, Chile: implications for arid watersheds affected by mining. *Journal of Geochemical*  
273 *Exploration*, 185, 33-51. <https://doi.org/10.1016/j.gexplo.2017.10.021>
- 274 Vargas, G., Ortlieb, L., Rutllant, J. (2000). *Aluviones históricos en Antofagasta y su relación con*  
275 *eventos El Niño/Oscilación del Sur*. *Revista geológica de Chile*, 27(2), 157-176.
- 276 Wilcox, A. C., C. Escauriaza, R. Agredano, E. Mignot, V. Zuazo, S. Otárola, L. Castro, J. Gironás, R.  
277 Cienfuegos, L. Mao. (2016). An integrated analysis of the March 2015 Atacama floods, *Geophys. Res.*  
278 *Lett.*, 43, 8035–8043. <https://doi.org/10.1002/2016GL069751>
- 279 **Statements and Declarations**
- 280 **Funding**  
281 Funding for this research was provided by the *Centre National d'Etudes Spatiales (CNES)*  
282 postdoctoral program to AC and KB, through the Programme National de Télédetection Spatiale  
283 (PNTS) project SECURITY, IRD-LMI-COPEM and ANID FONDECYT Iniciación Folio 11220285.
- 284 **Competing Interests**  
285 The authors have no interests to disclose.  
286



291 **Fig. 1 a.** Topographic map of northern Chile with transport network (white lines), main cities and towns  
292 (white dots). The towns of Sierra Gorda and Inca de Oro presented in panels 1d-e are indicated. Blue  
293 stars indicate UAV surveyed areas presented in Figure 2a-d. **b.** Rainfall accumulation between the 15-  
294 18<sup>th</sup> March 2022 retrieved from IMERG (V6). **c.** Interferometric coherence decrease based on images  
295 acquired on the descending track between 24<sup>th</sup> February and 31<sup>st</sup> May. Blue colours indicate stable  
296 surfaces (no difference from the mean pre-event coherence). Areas < -0.5 correspond to surfaces  
297 strongly impacted by flash floods and erosion processes, mostly localized in the drainage network,  
298 while areas between -0.5 and -0.2 may indicate strong transient coherence response due to moisture  
299 similar to that observed by Jordan et al. (2020), reflecting the rain cell extent. The Salar de Atacama  
300 salt flat was excluded from the field survey. **d.** Close up of Panel c showing the Inca de Oro site. Areas  
301 with a strong decrease in coherence and straight edges correspond to erosion and deposition within  
302 solar power plants (SPPs) under construction. **e.** Close up of Panel c showing the Sierra Gorda site.  
303 Grey areas in Panels d-e indicate masked areas of permanent coherence loss (mine tailings, solar  
304 power plants, towns, etc.). White arrows indicate flow direction

305

306



308 **Fig. 2 a-d.** Aerial views of selected study areas. Black arrows indicate flow direction. **a.** Inca de Oro  
 309 main road and avulsions of flash floods towards the NW. **b.** Piles of industrial waste at Inca de Oro  
 310 and unpaved road cuts after the passage of flash floods. **c.** Rilled hillslopes near El Salvador town. **d.**

311 Mudflow deposition within an alluvial fan. **e.** Ground evidence of unpaved road cuts in the Inca de Oro  
 312 area shown in figure 2b caused by stream and debris floods. **f.** Mudflows through an unpaved road  
 313 near Sierra Gorda. **g.** Downcutting of a stream flow channel that blocked an unpaved road. **h.**  
 314 Evidence of a mudflow using an unpaved road to flow. **i.** Example of mudflow deposition within an  
 315 ephemeral channel pool. **j.** Mudflow deposits near the main road that connects Sierra Gorda with  
 316 Antofagasta. **k.** Clay-pan area flooded one month after the rainfall event in the Sierra Gorda area

317

318

319

320

321

322 **Supplementary information Captions**

323 **SI-1** Sentinel-1 SLC images used in this study (acquired within the date range 20211102-20220531)

Region	Path/frame	Orbit
Sierra Gorda	156/668 149/1103	Descending Ascending
Taltal (central zone)	156/673 -	Descending -
Inca de Oro	156/678 47/1093	Descending Ascending

324